Vietnam Journal of Science and Technology ***64***(3) (2026) 473–485
DOI: https://doi.org/10.15625/2525-2518/18299

Preparation of activated carbons from coffee husk using KOH activation for phenol adsorption

Thi Thu Thuy Luong[1], Cu Dang Van[2], Huu Son Ta[1], Khu Le Van[1,*]

[1]*Faculty of Chemistry, Hanoi National University of Education, 136 Xuan Thuy Street, Cau Giay Ward, Ha Noi, Viet Nam*
[2]*Vietnam - Korea Institute of Science and Technology, Hoa Lac Hi-tech Park, Km 29 Thang Long Boulevard, Hoa Lac Ward, Ha Noi, Viet Nam*

[*]Email: *khulv@hnue.edu.vn*

Received: 26 April 2023; Accepted for publication: 24 January 2026

Abstract. This study explores the development of activated carbons (ACs) synthesized from coffee husks using potassium hydroxide (KOH) as the activating agent under varying conditions, focusing on their potential for phenol adsorption. The effects of impregnation ratio, activation temperature, and activation time on the pore structure and surface chemistry of the resulting ACs were studied. Under optimal synthesis conditions, the sample ACK3-750-60, with a specific surface area of 1905 $m^2 g^{-1}$, a total pore volume of 0.8613 $cm^3 g^{-1}$, and numerous surface functional groups (2.35 mmol g^{-1} acidic groups and 0.36 mmol g^{-1} basic groups), was obtained. The ACs have a predominantly microporous structure, as confirmed by iodine adsorption. The change in iodine number correlates with the pore texture obtained from BET measurements. Equilibrium sorption of phenol was studied and fitted by the Langmuir, Dubinin–Radushkevich, Elovich, and Temkin isotherms. The ACs achieved a maximum monolayer adsorption capacity of 199.20 mg g^{-1} at 30 °C, with an adsorption energy variation of 12.50 kJ mol^{-1}.

Keywords: coffee husk; activated carbon; surface area; phenol adsorption; isotherms.

Classification numbers: 2.4.2, 3.3.2, 3.4.2.

1. INTRODUCTION

In developing countries, economic development often entails many environmental consequences, especially water pollution. Phenol is the simplest phenolic compound that is commonly used in industries such as batteries, plastic, mining, textiles, electroplating, and petroleum. Phenol persists in the environment due to its low self-degradability and adversely affects aquatic flora, threatening the safety of drinking water, and has the potential to cause endocrine disruption and cancer in humans even at low concentrations [1]. Therefore, the National Technical Regulation on the quality of clean water for domestic use issued by the Vietnam Health Environment Management Agency requires that the concentration of phenol in drinking water must be below 1 μg L^{-1} (QCVN 01-1:2018/BYT). Several methods for phenol removal have been reported, including electrocoagulation, photocatalysis, coagulation/flocculation, adsorption, filtration, electrochemical oxidation, ion exchange, solvent extraction, advanced oxidation, membranes, and biodegradation [2, 3]. However, based on factors such as efficiency, cost,

operational features, design, and especially the treatment of phenol at low concentrations, adsorption remains the method with the greatest advantages.

Choosing the right adsorbent material is very important, especially when applied on an industrial scale. An ideal adsorbent material should possess key characteristics such as high adsorption capacity, strong selectivity, rapid adsorption/desorption kinetics, long life, abundant supply, and suitable price. As the world's second-largest coffee exporter, Viet Nam currently has a large surplus of coffee husk waste (CF) [4]. The main component of CF is cellulose, a particularly durable compound that completely decomposes in about 2 to 3 years under natural conditions. Recently, only a small amount of CF has been used as organic fertilizer or household heating material, while the remainder has been left untreated in coffee-growing areas. While it has a positive impact of softening the ground and limiting weeds, it can create a favorable environment for harmful microorganisms to grow. Therefore, it is necessary to have effective measures to use this surplus coffee husk. With its high carbon content [5], the CF can be a cost-effective raw material for producing activated carbon, a well-known adsorbent. The preparation of activated carbons from biomass has been extensively investigated. Chemical activation methods are particularly effective, as they require lower temperatures and shorter processing times [6] than physical activation, while yielding superior pore structures [7]. Among widely used chemical activators, such as alkaline hydroxides, zinc chloride, phosphoric acid, etc., potassium hydroxide (KOH) has the advantage of creating micropores [8] and –OH functional groups on the carbon surface [9], enhancing the adsorption capability for small molecules.

In this work, the relationship between activated carbon preparation and its phenol adsorption ability was investigated. The effects of KOH:biochar ratio, activation temperature, and activation time were studied to determine the optimal parameters for producing activated carbons with advanced porosity and high phenol adsorption efficiency.

2. MATERIALS AND METHODS

2.1. Materials

Arabica coffee husks were sourced from a coffee mill in Son La Province, Viet Nam. The husks were thoroughly washed with water, dried at 110 °C for 12 hours, crushed into smaller pieces, and sieved to achieve a 1.0 mm particle size. The chemical composition of the CF particles, as determined by energy dispersive X-ray spectroscopy (EDX), was found to be: C: 49.38 %, O: 45.30 %, Mg: 0.18 %, Al: 0.23 %, Si: 0.31 %, P: 0.14 %, S: 0.28 %, Cl: 0.08 %, K: 3.50 %, Ca: 0.60 % by mass (not shown). Phenol crystals (purity > 99 %) and potassium hydroxides (purity 85 %) were purchased from Xylong Chemical, China. A stock solution of phenol at a concentration of 1000 mg L^{-1} was prepared two hours before use and was subsequently diluted to the desired concentrations without pH adjustment.

2.2. Preparation of activated carbon

CF powder was subjected to carbonization at 450 °C for 90 minutes with a heating rate of 20 °C min^{-1} under a nitrogen flow of 300 mL min^{-1}. The resulting biochars were impregnated with sufficient amounts of KOH (KOH:biochars mass ratio varied from 1:1 to 4:1). After drying at 120 °C for 12 hours, they were then heated in a nitrogen atmosphere (300 mL min^{-1}) at 400 °C for 20 min. Activation was conducted by gradually increasing the temperature (10 °C min^{-1}) to target levels between 650 and 800 °C, followed by a predetermined retention time of 40 to 100 min.

After that, it was neutralized by 0.1 N HCl, washed with hot water until the pH stabilized in the range of 6.6 to 7.0, and finally dried in a vacuum oven at 120 °C for 24 hours. The activated carbons (ACs) were labeled as ACK a-b-c, in which "a" stands for KOH:biochars mass ratio, "b" - activation temperature, and "c" - activation time.

2.3. Characterization

The textural properties of the ACs were analyzed by BET (Micromeritics TriStar 3020). The functional groups were identified via FTIR (Nicolet, Nexus 670). Morphological information was obtained using FE-SEM (S4800-Hitachi). Acidic and basic functional groups were determined by the Boehm method [10]. The adsorption capacity was determined using the iodine number (ASTM D 4607-4). The carbon yield was calculated using the formula:

$$Y = \frac{W_f}{W_0} \times 100 \quad (1)$$

where Y presents the carbon yield, W_f and W_0 are the weights of activated carbon and of the initial coffee husks. Phenol adsorption was conducted with phenol concentration of 45-250 mg L^{-1} and 100 mg AC (particle size $0.15 < d < 0.30$ mm) after being agitated at 120 rpm for 24 hours at 30 °C. The equilibrium concentration of phenol was analyzed following the procedure outlined in the Standards Methods for the Examination of Water and Wastewater, published by the American Public Health Association (APHA). Each experiment was carried out in triplicate to ensure reliability. The equilibrium adsorption capacity, q_e (mg g^{-1}), was determined using the equation:

$$q_e = \frac{(C_o - C_e)V}{m} \quad (2)$$

where C_o and C_e (mg L^{-1}) are the initial and equilibrium concentrations of phenol, V (L) is the volume of the solution, and m (g) is the dosage of activated carbon used.

3. RESULTS AND DISCUSSION

3.1. Characterization of activated carbons

The carbon yield results for the preparation of ACs under various conditions are summarized in Table 1. The efficiency of AC synthesis from coffee husks ranges from 27.5 to 35.1 %. It was noted that increasing the KOH:biochar ratio, activation time, and activation temperature gradually reduces the efficiency of AC production. This can be attributed to the enhanced interaction between carbon and KOH during the activation process, which consumes a portion of carbon and facilitates the release of volatiles from the material. A comparable trend was also reported by Njewa J.B. when preparing activated carbon from agro-waste [11].

The nitrogen adsorption-desorption isotherms of ACs elaborated from coffee husk prepared under varying conditions are illustrated in Figure 1. The shapes of these isotherms conform to Type I classification according to IUPAC standards, with no hysteresis observed at $p/p° > 0.42$, indicating that all synthesized ACs are predominantly microporous. This is confirmed by the textural data for ACs calculated from the isotherms shown in Table 1, which indicate that micropores account for over 98 % of the specific surface area and more than 93 % of the total pore volume. These results align with other studies, indicating that KOH activation led to a high percentage of micropores [12, 13]. The textural characteristics of all studied activated carbons

surpass those of Tra Bac activated carbon – a commercialized type made from coconut shells widely used in Viet Nam, which exhibits a surface area of 691 m^2 g^{-1} and a pore volume of 0.159 mL g^{-1} [14]. According to the findings, the impregnation ratio showed the greatest impact on the pore structure of AC. S_{BET} increases drastically from 838 to 1905 m^2 g^{-1} when the impregnation ratio increases from 1:1 to 3:1 but decreases to 1694 m^2 g^{-1} when the impregnation ratio further increases to 4:1. The total pore volume also follows a comparable trend, increasing from 0.3915 to 0.8613, then decreasing to 0.7742 cm^3 when the impregnation ratio increases from 1:1 to 3:1 and then to 4:1. The increase in the activating agent promotes the contact area between coffee husk precursors and KOH, and sequentially promoting micropore formation and enlarging the specific surface area of carbon [15]. In contrast, further increasing the KOH concentration to an impregnation ratio of 4:1 appears to degrade the deeper structure of the aromatic layer, leading to pore enlargement and reductions in both S_{BET} and total pore volume [16].

At a fixed KOH:biochar ratio of 3:1, the biochars were activated from 650 to 800 °C to investigate the impact of activation temperature. As shown in Figure 1(b), nitrogen uptake at 77 K reached its peak at an activation temperature of 750 °C. Pore development improved within this temperature range, with S_{BET} increasing from 1216 to 1905 m^2 g^{-1} as temperatures rose from 650 to 750 °C. However, at temperatures exceeding 752 °C (the boiling point of metal K), metal K vaporized and migrated between carbon microcrystals. This process destroyed the aromatic lamellar layer and expanded pore sizes [16], thereby decreasing microporosity. At 800 °C, the specific surface area and total pore volume decreased to 1740 m^2 g^{-1} and 0.8020 cm^3 g^{-1}, respectively.

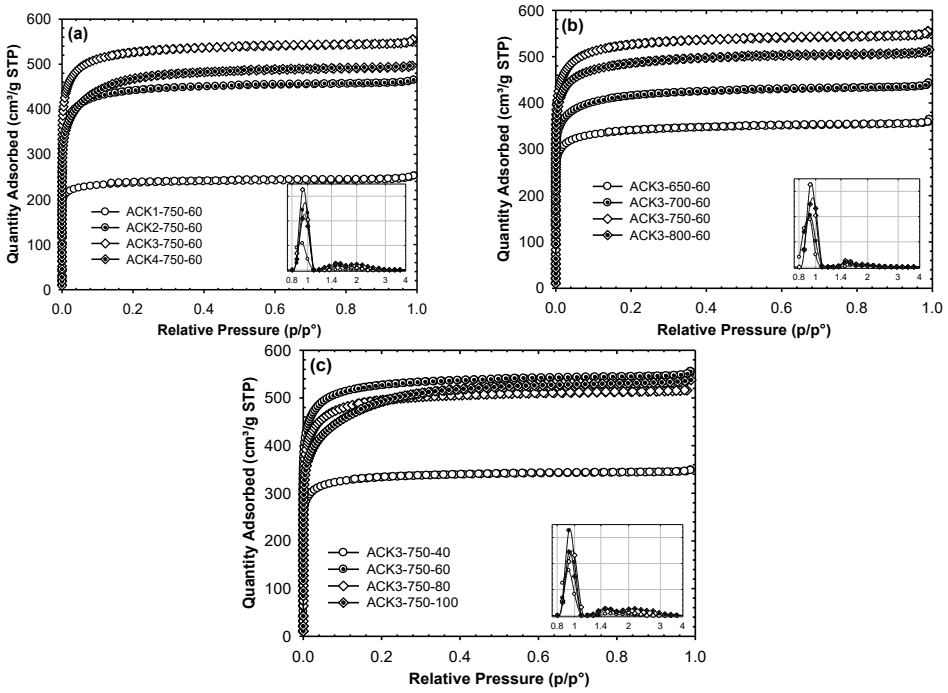

Figure 1. Adsorption-desorption isotherms of N_2 and pore-size distribution curves (inserted images) of ACs by KOH activation at different: (a) impregnation ratios, (b) activation temperatures, and (c) activation times.

The pore development of ACs is least affected by the activation time. After 40 minutes of activation, the pores are not fully developed, with S_{BET} and V_{total} remaining significantly lower

compared to other activation times, reaching only 1201 m^2 g^{-1} and 0.5402 cm^3 g^{-1}, respectively. When the activation time is 60 min, the S_{BET} and V_{total} increase significantly to 1905 m^2 g^{-1} and 0.8613 cm^3 g^{-1}, respectively. However, further prolonging the activation time to 80 and 100 minutes results in only a marginal decline in these values. Specifically, at 100 minutes of activation, the S_{BET} of the resulting activated carbon decreases to 1786 m^2 g^{-1}, and V_{total} drops to 0.8194 cm^3 g^{-1}. This might stem from prolonged reaction between KOH and carbon, leading to pore widening and collapse. Comparable trends in pore structure variation due to activation time have been found in the ACs prepared from other agricultural by-products [17]. The inserted images of pore size distributions (PSDs) illustrate that all samples predominantly feature pores smaller than 4.0 nm, with the majority in the 0.8-2.0 nm range. These findings align with data derived from N_2 adsorption-desorption isotherms.

Table 1. Porosity characteristics, carbon yield, and iodine number of the activated carbon samples.

Label	S_{BET} (m^2 g^{-1})	S_{mic} (m^2 g^{-1})	S_{mic}/S_{BET} (%)	V_{mic} (cm^3 g^{-1})	V_{tot} (cm^3 g^{-1})	V_{mic}/V_{tot} (%)	Y (%)	Iodin number (mg g^{-1})
ACK1-750-60	838	827	98.69	0.3645	0.3915	93.10	35.11	840
ACK2-750-60	1587	1561	98.36	0.6820	0.7227	94.37	32.32	1549
ACK3-750-60	1905	1891	99.27	0.8252	0.8613	95.81	30.74	1850
ACK4-750-60	1694	1667	98.41	0.7327	0.7742	94.64	29.23	1652
ACK3-650-60	1216	1198	98.52	0.5281	0.5574	94.74	34.47	1210
ACK3-700-60	1492	1470	98.53	0.6468	0.6904	93.68	31.56	1447
ACK3-800-60	1740	1721	98.91	0.7615	0.8020	94.95	27.52	1700
ACK3-750-40	1201	1188	98.92	0.5178	0.5402	95.86	32.48	1195
ACK3-750-80	1789	1767	98.77	0.7721	0.8028	96.18	29.77	1718
ACK3-750-100	1786	1761	98.60	0.7723	0.8194	94.25	28.13	1710

The iodine number for ACs prepared under varying conditions presented in Table 1 reveals a clear correlation among the S_{BET}, S_{mic}, and iodine number. Notably, the impregnation ratio has the greatest effect on S_{BET}, S_{mic}, and iodine number. The iodine number increases from 840 to 1850 mg g^{-1} as the impregnation ratio rises from 1:1 to 3:1, but decreases to 1652 mg g^{-1} when the ratio reaches 4:1. Regarding activation temperature, the iodine number grows from 1210 to 1850 mg g^{-1} as the temperature increases from 650 to 750 °C, but decreases to 1700 mg g^{-1} at 800 °C. Iodine number increases with activation time up to 60 min, then decreases as activation time increases to 80 and 100 min. The iodine number characterizes the adsorption ability and microporosity of activated carbon and is comparable to S_{BET} [18]. Based on the S_{BET}, S_{mic}, and iodine number values, it can be concluded that the micropores of the as-prepared ACs serve as active sites and can be employed for adsorption.

The morphology of ACs synthesized under varying conditions was examined by FE-SEM. Figure 2 highlights the influence of different impregnation ratios on the textural properties of the resulting activated carbon. At an impregnation ratio of 1:1, activated carbon has an uneven and rather packed surface with small cavities and some open pores. As the ratio increases to 2:1 and 3:1, small cracks develop into larger, deeper pores. This might be due to increased interaction between KOH and C, leading to a highly porous structure with many caves and cavities, as suggested by BET measurements. However, at a higher impregnation ratio of 4:1, the violent interaction between the activation agent and carbon destroyed the freshly formed pores, resulting in a flatter surface of the AC samples.

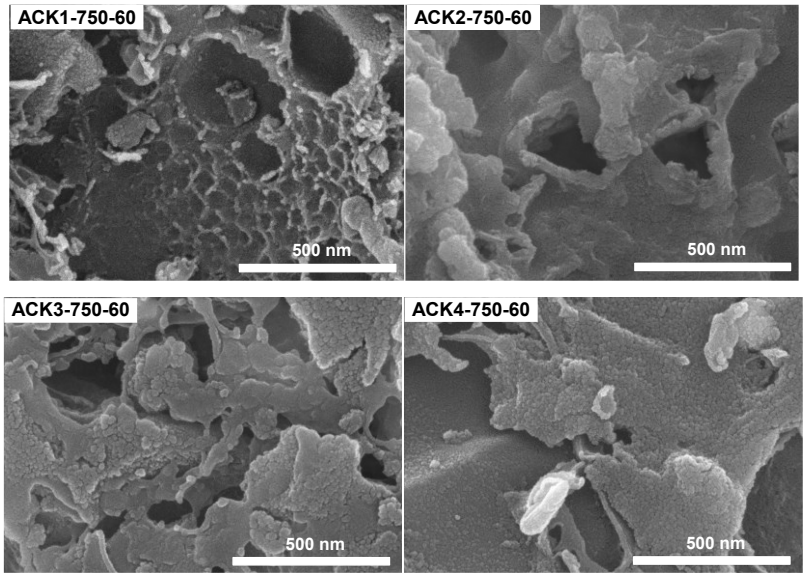

Figure 2. FE-SEM images of the ACs at varying impregnation ratios.

FTIR spectroscopy was utilized to determine the surface functional groups on the ACs, as shown in Figure 3. The band at 3410 cm^{-1} is customarily assigned to the O–H stretching bond [19]. The band around 3000-2800 cm^{-1} was due to symmetric and asymmetric stretching of C–H in –CH, $–CH_2$, or $–CH_3$ [20]. The band at 2858 cm^{-1} is assigned to the vibration of the CH_3-O group. These bands are almost unchanged under different activation conditions. The band appearing at 1680 cm^{-1} is associated with C=O vibrations of acidic groups [21], while the band at 1545 cm^{-1} is ascribed to carboxylate ion groups. This band decreases with increasing impregnation ratio and activation temperature, indicating a decrease in carboxylate content. The broadband around 1057 cm^{-1} corresponds to C–O stretching vibrations found in primary C–OH [17].

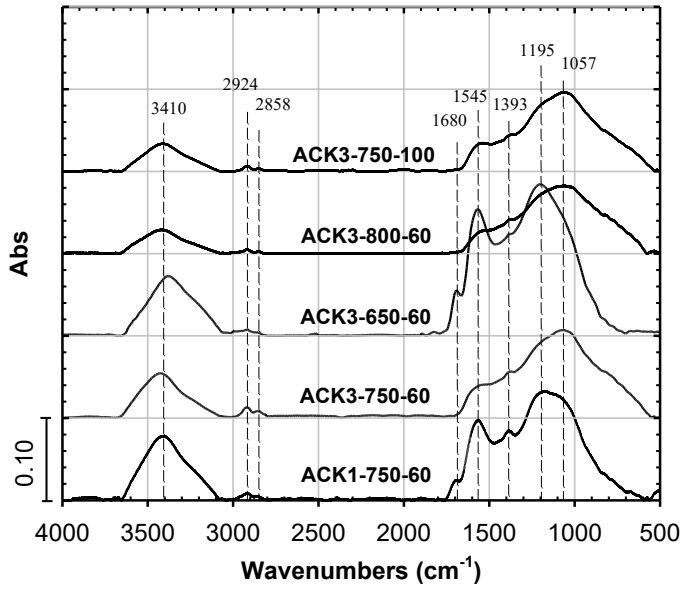

Figure 3. FTIR spectra of some selected AC samples.

The surface functional groups on the ACs under study are quantified using Boehm titration techniques. Total acidic and basic groups and their respective ratios are summarized in Table 2. The acidic groups, falling between 1.73 and 2.35 mmol g^{-1}, consistently outnumber basic groups, which range from 0.36 to 0.86 mmol g^{-1} across all samples. The ratio of acidic to basic groups is notably high, exceeding 2.5 in all cases. Except for the ACK2-750-60 and ACK3-700-60 samples, which have high ratios of 6.53 and 5.76, respectively, the remaining samples have ratios ranging from 2.58 to 4.35. It can also be seen that the amounts of acidic groups gradually decrease at elevated temperatures, especially the carboxyl group, while the amounts of basic groups remain relatively constant. This might be because the basic groups are more thermostable than the acidic groups: quinone and carbonyl decompose above 700 °C, while carboxyl groups decarboxylation to form CO_2 at below 400 °C, phenol groups release CO between 500-750 °C, and lactone break downs to form CO above 600 °C [22]. Accordingly, the amount of carboxyl groups is most affected, consistent with the FT-IR results.

Table 2. Surface groups of the AC samples.

Label	Surface functional groups (mmol g^{-1})					Acidic groups/ Basic groups
	Carboxyls	Lactones	Phenols	Total acidic groups	Total basic groups	
ACK1-750-60	0.96	0.58	0.47	2.01	0.48	4.19
ACK2-750-60	1.00	0.59	0.76	2.35	0.36	6.53
ACK3-750-60	0.75	0.31	0.67	1.73	0.67	2.58
ACK4-750-60	0.67	0.63	0.70	2.00	0.46	4.35
ACK3-650-60	1.07	0.50	0.66	2.23	0.86	2.59
ACK3-700-60	0.98	0.53	0.68	2.19	0.38	5.76
ACK3-800-60	0.48	0.49	0.53	1.50	0.37	4.05
ACK3-750-40	0.86	0.47	0.53	1.86	0.69	2.70
ACK3-750-80	0.84	0.43	0.98	2.25	0.57	3.95
ACK3-750-100	0.74	0.55	0.45	1.74	0.46	3.78

3.2. Phenol adsorption

To evaluate the phenol adsorption capacity of the ACs, BET analysis and FTIR spectroscopy were performed on two representative samples prepared at 700 °C and 750 °C, respectively, and subsequently immersed in a phenol solution of 150 mg L^{-1} (labeled as ACK3-700-60-Phenol and ACK3-750-60-Phenol). A comparison of the N_2 adsorption-desorption isotherms obtained before and after immersion in the phenol solution (Figure 4(a)) revealed a notable reduction in the amount of N_2 adsorbed by the sample after immersion. This decrease resulted in a significant drop in the specific surface area, particularly affecting the micropore areas (S_{mic} from 1470 to 1137 m^2 g^{-1} for ACK3-700-60, and from 1891 to 1603 m^2 g^{-1} for ACK3-750-60). Furthermore, an analysis of the FTIR spectra (Figure 4(b)) identified three new bands with strong intensities in the samples after phenol immersion. The band at 1706 cm^{-1} is attributed to the stretching vibration of C=C functional groups, while the one at 1550 cm^{-1} corresponds to the C=C stretching vibrations associated with the aromatic ring [23]. Additionally, the fingerprint region around 515 cm^{-1} displays various complex absorptions attributed to C-O, C-C, and C-H bending vibrations [24]. The findings from the BET and FTIR analyses validated the effective adsorption of phenol onto the activated carbon surface, highlighting the significant role of the micropores in this process.

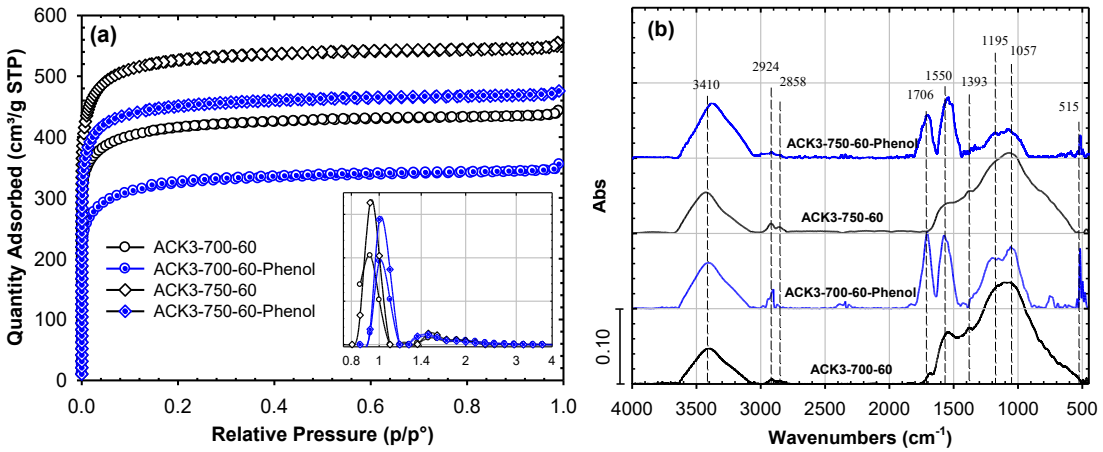

Figure 4. (a) Adsorption-desorption isotherms of N_2 at 77K and (b) FTIR spectra of ACs produced at 700 and 750 °C before and after phenol adsorption.

The adsorption equilibrium isotherms of phenol at 30 °C of the samples prepared at different impregnation ratios and activation temperatures are given in Figure 5 by plotting q_e against C_e. As can be seen, q_e increases with C_e, initially significantly and then more slowly. Since there are no plateaus, it can be inferred that under the investigated conditions, the adsorption is not saturated. Within the investigated concentration range, the ACK3-750-60 sample consistently exhibited the highest adsorption capacities, likely due to its enhanced surface area and pore volume.

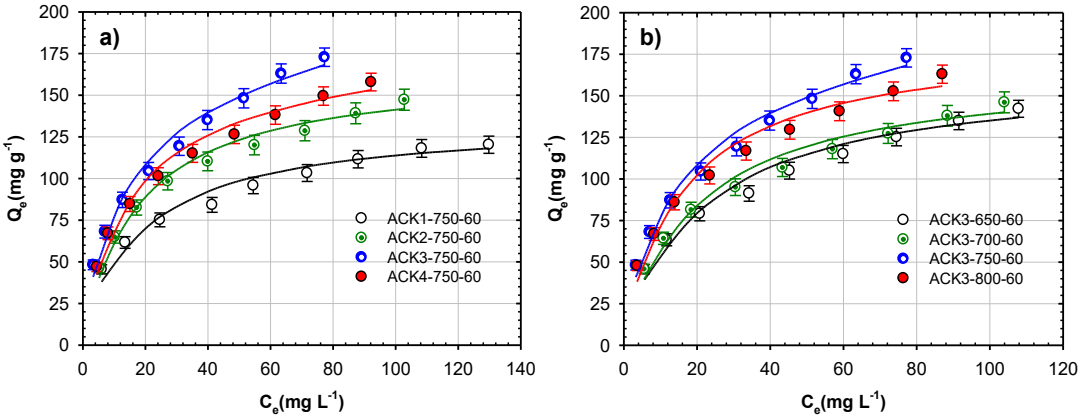

Figure 5. Adsorption isotherms of phenol at 30 °C on AC samples synthesized at different: (a) impregnation ratios, (b) activation temperatures.

To model the adsorption behavior more comprehensively, four isotherm models, namely Langmuir (Eq. (3)), Dubinin–Radushkevich (Eq. (4)), Elovich (Eq. (5)), and Temkin (Eq. (6)) [25], were employed to fit the experimental equilibrium concentration of phenol in the solution. The mathematical expressions for these models are listed below:

$$\frac{C_e}{q_e} = \frac{1}{q_m} C_e + \frac{1}{q_m K_L} \tag{3}$$

$$\ln q_e = \ln q_m - \beta\varepsilon^2 \tag{4}$$

$$\ln \frac{q_e}{C_e} = -\frac{q_e}{q_{mE}} + \ln K_E q_m \tag{5}$$

$$q_e = B \ln K_T + B \ln C_e \tag{6}$$

where q_m represents the maximum coverage adsorption capacity, ε is Polani potential in the Dubinin–Radushkevich equation. K_L, β, K_E, B, and K_T are the constants of the four models.

The correlation between the empirical and predicted adsorption values was estimated using the coefficient of determination (R^2). Table 3 summarizes the modeled parameters along with their respective R^2 values. The Dubinin–Radushkevich isotherm exhibited a low R^2 (≤0.7795). The Elovich isotherm, although it has a rather high R^2 ($0.9770 \leq R^2 \leq 0.9958$), yields calculated maximum monolayer coverage capacities (q_m) that are considerably lower than the experimental adsorbed amounts (at the highest C_e of each sample). Therefore, the Dubinin–Radushkevich and Elovich models are not suitable for describing phenol adsorption onto activated carbon under the conditions investigated. Both adsorption models, Langmuir and Temkin, yield R^2 values close to 1 ($0.9813 \leq R^2 \leq 0.9930$ for Langmuir and $0.9742 \leq R^2 \leq 0.9957$ for Temkin), indicating excellent linearity, confirming that both models can describe the adsorption of phenol on the obtained ACs.

Table 3. Equilibrium parameters for phenol adsorption onto ACs.

	Dubinin–Radushkevich	Elovich		Tempkin		Langmuir			
	R^2	q_m (mg g^{-1})	R^2	B (mg g^{-1})	R^2	q_m (mg g^{-1})	R^2	$R_{L.max}$	$R_{L,min}$
ACK1-750-60	0.7128	37.49	0.9856	25.18	0.9856	134.95	0.9909	0.292	0.069
ACK2-750-60	0.7677	53.33	0.9957	33.39	0.9957	165.73	0.9930	0.277	0.065
ACK3-750-60	0.6989	67.66	0.9742	39.62	0.9742	199.20	0.9813	0.261	0.060
ACK4-750-60	0.7795	58.73	0.9923	36.06	0.9923	179.24	0.9907	0.267	0.062
ACK3-650-60	0.7185	53.79	0.9809	32.80	0.9809	163.93	0.9855	0.321	0.078
ACK3-700-60	0.7556	54.67	0.9894	33.61	0.9894	166.56	0.9887	0.303	0.073
ACK3-800-60	0.6972	59.50	0.9839	36.36	0.9839	184.23	0.9873	0.261	0.060

For the Langmuir model, the separation factor R_L is also a crucial parameter to indicate the type of adsorption, in which $0 < R_L < 1$ implies favorable adsorption. R_L is calculated as follows:

$$R_L = \frac{1}{1 + K_L C_o} \tag{7}$$

where K_L is the Langmuir constant, and C_o is the initial concentration of phenol in the solution.

Table 3 shows that all $R_{L,min}$ and $R_{L,max}$ values calculated at the minimum and maximum C_o values for all ACs fall within the range of 0 to 1, indicating favorable phenol adsorption. Based on the $R_{L,max}$, $R_{L,min}$, and R^2 criteria, the Langmuir model can appropriately describe the adsorption data. Therefore, for convenience in comparison with other authors, data from the Langmuir model will be used for further discussion. It can also be observed from the Table 3 that the maximum adsorption capacity q_m obtained from the Langmuir isotherm is reported to range between 134.95 and 199.20 mg g^{-1} and can be compared to q_m values of activated carbon from magnetic chitosan (51.68 mg g^{-1}) [26], coconut tree waste (56.00 mg g^{-1}) [27], black wattle bark waste (98.57 mg g^{-1}) [28], rice husk (194.24 mg g^{-1}) [29], as well as Chinese commercial activated

carbon (169.91 to 212.96 mg g^{-1}) [30]. The differences in q_m of ACs prepared from coffee husks under different conditions can be attributed to variations in surface area and pore texture, particularly micropore volume. The ACs with large microporous volume groups will have high phenol adsorption capacity, as maximum adsorption capacity is generally a linear function of micropore volume [31].

In this study, the plot of q_m (of Langmuir) versus V_{mic} (in Table 1) shows a nearly linear relationship, as shown in Figure 6. ACK3-650-60 and ACK3-750-60 samples show positive deviation (higher phenol adsorption capacities), while the ACK3-700-60 and ACK2-750-60 samples display negative deviation (lower phenol adsorption capacities). Apart from the surface area, surface functional groups also strongly influence phenol adsorption; acidic groups have a reduced effect, while basic groups enhance adsorption. Thus, the acidic-to-basic group ratio effectively measures the contribution of surface functionality to phenol adsorption. The ACK3-650-60 and ACK3-750-60 samples that have a smaller ratio of acidic/basic groups (2.6) will have a larger q_m, and the ACK3-700-60 and ACK2-750-60 samples that have a higher ratio of acidic/basic groups (5.8 and 6.5, respectively), will have a lower q_m. Consequently, some empirical data lie above or below the q_m-V_{mic} plot in Figure 6.

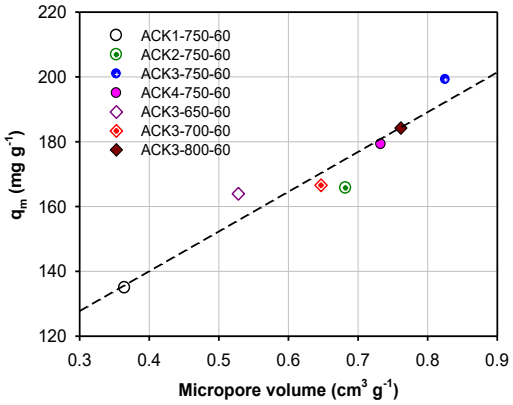

Figure 6. Relationship between the maximum monolayer coverage capacity and the micropore volume for the ACs produced at different activation conditions.

As indicated above, under these experimental conditions, the Temkin model is suitable for describing the experimental data within a moderate error limit. Therefore, this model is adopted to calculate the variation of adsorption energy. In the Temkin model, B is the constant related to the heat of adsorption given by the following equation [32]:

$$B = \frac{q_m RT}{\Delta Q} \tag{8}$$

where q_m (mg g^{-1}) is the maximum monolayer coverage capacity; R (J mol^{-1} K^{-1}) is the gas constant, T (K) is the temperature, and ΔQ (J mol^{-1}) is a variation of adsorption energy. The q_m can be obtained either by the Langmuir isotherm or calculated from specific surface area (S_{BET}) using the following formula:

$$q_m = \frac{S_{BET} M}{\sigma N_A} \tag{9}$$

where σ is the surface area of the phenol molecule (30.49×10^{-20} m^2 [32]), N_A is Avogadro's constant (6.02×10^{23} mol^{-1}), M is the molar mass of phenol (94.11 g mol^{-1}), and S_{BET} is the specific surface area (m^2 g^{-1}).

Table 4. q_m and ΔQ for the adsorption of phenol onto activated carbon.

Sample	q_m calculated using BET surface area (mg g^{-1})	ΔQ (kJ mol^{-1})	q_m determined using Langmuir equation (mg g^{-1})	ΔQ (kJ mol^{-1})
ACK1-750-60	429.66	42.99	134.95	13.50
ACK2-750-60	813.69	61.39	165.73	12.50
ACK3-750-60	976.74	62.10	199.20	12.66
ACK4-750-60	868.55	60.68	179.24	12.52
ACK3-650-60	623.47	47.88	163.93	12.59
ACK3-700-60	764.98	57.33	166.56	12.48
ACK3-800-60	892.14	61.82	184.23	12.77

The ΔQ values calculated by equation (10) for both q_m from the Langmuir isotherm and S_{BET} are presented in Table 4. These results reveal that all calculated ΔQ values are positive, indicating the exothermic nature of the phenol adsorption process. Notably, the ΔQ values based on q_m from S_{BET} are always 4 to 5 times greater than those obtained via Langmuir-derived q_m. This is because the assumption that all BET surfaces are covered by phenol molecules is practically impossible. Therefore, the ΔQ values based on q_m from the Langmuir isotherm are closer to empirical data. Except for the ACK1-750-60 sample with ΔQ = 13.50 kJ mol^{-1}, all other ACs have ΔQ ≈ 12.50 kJ mol^{-1}. This finding is relatively similar to a previous research by Hamdaoui and Naffrechoux, who reported a ΔQ value of 12.16 kJ mol^{-1} [32] for phenol adsorption on commercially available granular activated carbon.

4. CONCLUSIONS

Activated carbons from coffee husks were successfully synthesized using a two-step KOH activation under different conditions. The results revealed that the KOH:biochar impregnation ratio was the most critical parameter, and the optimal preparation conditions for obtaining activated carbon with a large specific surface area and predominantly microporous particles were a KOH:biochar mass ratio of 3:1, an activation temperature of 750 °C, and an activation time of 60 min. Under these conditions, the resulting activated carbon exhibited a S_{BET} of 1905 m^2 g^{-1}, a V_{mic} of 1891 m^2 g^{-1}, a V_{total} of 0.8613 cm^3 g^{-1}, and an iodine number of 1850 mg g^{-1}. The adsorption behavior of phenol was modeled using the Langmuir, Dubinin–Radushkevich, Elovich, and Temkin isotherms. Based on the Langmuir model, the AC prepared under these optimized conditions demonstrated a phenol adsorption capacity of 199.20 mg g^{-1}. These experimental findings demonstrate that producing AC from coffee husk waste is a cost-effective and sustainable approach for wastewater treatment applications in Viet Nam.

CRediT authorship contribution statement. Thi Thu Thuy Luong: Formal analysis. Cu Dang Van: Investigation. Huu Son Ta: Investigation. Khu Le Van: Methodology, Supervision.

Declaration of competing interest. The authors declare that they have no known competing financial interests or personal relationships that could have appeared to influence the work reported in this paper.

REFERENCES

1. Panigrahy N., Priyadarshini A., Sahoo M. M., Verma A. K., Daverey A., Sahoo N. K. – A comprehensive review on eco-toxicity and biodegradation of phenolics: Recent progress and future outlook. Environ. Technol. Innov., **27** (2022) 102423. https://doi.org/10.1016/j.eti.2022.102423.
2. Grace Pavithra K., Sundar Rajan P., Arun J., Brindhadevi K., Hoang Le Q., Pugazhendhi A. – A review on recent advancements in extraction, removal and recovery of phenols from phenolic wastewater: Challenges and future outlook. Environ. Res., **237** (2023) 117005. https://doi.org/10.1016/j.envres.2023.117005.
3. Saputera W. H., Putrie A. S., Esmailpour A. A., Sasongko D., Suendo V., Mukti R. R. – Technology advances in phenol removals: Current progress and future perspectives. Catalysts, **11** (2021) 998. https://doi.org/10.3390/catal11080998.
4. Nam N. H., Ngoc C. T. A., Van Bay T. – Investigation on gasification of coffee husk in CO_2, H_2O, and mixed atmospheres. Vietnam J. Chem., **59** (2021) 775–780. https://doi.org/10.1002/vjch.202100002.
5. Thuy Luong Thi T., Ta H. S., Le Van K. – Activated carbons from coffee husk: Preparation, characterization, and reactive red 195 adsorption. J. Chem. Res., **45** (2020) 380–394. https://doi.org/10.1177/1747519820970469.
6. Siipola V., Tamminen T., Källi A., et al. – Effects of biomass type, carbonization process, and activation method on the properties of bio-based activated carbons. BioResources, **13** (2018) 5976–6002. https://doi.org/10.15376/biores.13.3.5976-6002.
7. Sharma G., Sharma S., Kumar A., et al. – Activated carbon as superadsorbent and sustainable material for diverse application. Adsorp. Sci. Technol., **2022** (2022) 4184809. https://doi.org/10.1155/2022/4184809.
8. Zhang Y., Zhao Y.-P., Qiu L.-L., et al. – Insights into the KOH activation parameters in the preparation of corncob-based microporous carbon for high-performance supercapacitors. Diamond Relat. Mater., **129** (2022) 109331. https://doi.org/10.1016/j.diamond.2022.109331.
9. Oginni O., Singh K., Oporto G., Dawson-Andoh B., McDonald L., Sabolsky E. – Influence of one-step and two-step KOH activation on activated carbon characteristics. Bioresour. Technol. Rep., **7** (2019) 100266. https://doi.org/10.1016/j.biteb.2019.100266.
10. Schönherr J., Buchheim J., Scholz P., Adelhelm P. – Boehm titration revisited (Part I): Practical aspects for achieving a high precision in quantifying oxygen-containing surface groups on carbon materials. C, **4** (2018) 21. https://doi.org/10.3390/c4020021.
11. Njewa J. B., Vunain E., Biswick T. – Synthesis and characterization of activated carbons prepared from agro-wastes by chemical activation. J. Chem., **2022** (2022) 1–13. https://doi.org/10.1155/2022/9975444.
12. Thongpat W., Taweekun J., Maliwan K. – Synthesis and characterization of microporous activated carbon from rubberwood by chemical activation with KOH. Carbon Lett., **31** (2021) 1079–1088. https://doi.org/10.1007/s42823-020-00224-z.
13. Guo Y., Wang Q. – Fabrication and characterization of activated carbon from *Phyllostachys edulis* using single-step KOH activation with different temperatures. Processes, **10** (2022) 1712. https://doi.org/10.3390/pr10091712.
14. Van H. T., Bui T. T. P., Nguyen L. H. – Residual organic compound removal from aqueous solution using commercial coconut shell activated carbon modified by a mixture of seven metal salts. Water Air Soil Pollut., **229** (2018) 292. https://doi.org/10.1007/s11270-018-3953-4.
15. Nandi R., Jha M. K., Guchhait S. K., Sutradhar D., Yadav S. – Impact of KOH activation on rice husk derived porous activated carbon for carbon capture at flue gas alike temperatures with high CO_2/N_2 selectivity. ACS Omega, **8** (2023) 4802–4812. https://doi.org/10.1021/acsomega.2c06955.
16. Liu P., Sun S., Huang S., et al. – KOH activation mechanism in the preparation of brewer's spent grain-based activated carbons. Catalysts, **14** (2024) 814. https://doi.org/10.3390/catal14110814.
17. Zhang Y.-J., Xing Z.-J., Duan Z.-K., Li M., Wang Y. – Effects of steam activation on the pore structure and surface chemistry of activated carbon derived from bamboo waste. Appl. Surf. Sci., **315** (2014) 279–286. https://doi.org/10.1016/j.apsusc.2014.07.126.

18. Anisuzzaman S. M., Sinring N., Fran Mansa R. – Properties tuning of palm kernel shell biochar granular activated carbon using response surface methodology for removal of methylene blue. J. Appl. Sci. Process Eng., **8** (2021) 1002–1019. https://doi.org/10.33736/jaspe.3961.2021.
19. Ilić M., Haegel F.-H., Lolić A., et al. – Surface functional groups and degree of carbonization of selected chars from different processes and feedstock. PLoS One, **17** (2022) e0277365. https://doi.org/10.1371/journal.pone.0277365.
20. Angın D., Altintig E., Köse T. E. – Influence of process parameters on the surface and chemical properties of activated carbon obtained from biochar by chemical activation. Bioresour. Technol., **148** (2013) 542–549. https://doi.org/10.1016/j.biortech.2013.08.164.
21. de Souza C. C., de Souza L. Z. M., Yılmaz M., et al. – Activated carbon of *Coriandrum sativum* for adsorption of methylene blue: Equilibrium and kinetic modeling. Cleaner Mater., **3** (2022) 100052. https://doi.org/10.1016/j.clema.2022.100052.
22. Rocha R. P., Pereira M. F. R., Figueiredo J. L. – Characterisation of the surface chemistry of carbon materials by temperature-programmed desorption: An assessment. Catal. Today, **418** (2023) 114136. https://doi.org/10.1016/j.cattod.2023.114136.
23. Fairus M. J. M., Ibrahim M. F., Zainal N. H., Abd-Aziz S., Phang L.-Y. – Phenol adsorption performance by bamboo activated carbon produced using fabricated two-in-one carbonization activation pilot reactor. Environ. Technol. Innov., **40** (2025) 104427. https://doi.org/10.1016/j.eti.2025.104427.
24. Thummajitsakul S., Piyaphan P., Khamthong S., Unkam M., Silprasit K. – Comparison of PTIR fingerprint, phenolic content, antioxidant and anti-glucosidase activities among *Phaseolus vulgaris* L., *Arachis hypogaea* L. and *Plukenetia volubilis* L. Electron. J. Biotechnol., **61** (2023) 14–23. https://doi.org/10.1016/j.ejbt.2022.10.003.
25. Ayawei N., Ebelegi A. N., Wankasi D. – Modelling and interpretation of adsorption isotherms. J. Chem., **2017** (2017) 1–11. https://doi.org/10.1155/2017/3039817.
26. Salari M., Dehghani M. H., Azari A., Motevalli M. D., Shabanloo A., Ali I. – High performance removal of phenol from aqueous solution by magnetic chitosan based on response surface methodology and genetic algorithm. J. Mol. Liq., **285** (2019) 146–157. https://doi.org/10.1016/j.molliq.2019.04.065.
27. Duarte M., Nascimento G., Santos M., et al. – Adsorption of phenol on adsorbents produced from coconut tree waste: Kinetic and equilibrium studies. Environ. Eng. Manag. J., **18** (2019) 693–705. https://doi.org/10.30638/eemj.2019.063.
28. Lütke S. F., Igansi A. V., Pegoraro L., Dotto G. L., Pinto L. A. A., Cadaval T. R. S. – Preparation of activated carbon from black wattle bark waste and its application for phenol adsorption. J. Environ. Chem. Eng., **7** (2019) 103396. https://doi.org/10.1016/j.jece.2019.103396.
29. Lv S., Li C., Mi J., Meng H. – A functional activated carbon for efficient adsorption of phenol derived from pyrolysis of rice husk, KOH-activation and EDTA-4Na-modification. Appl. Surf. Sci., **510** (2020) 145425. https://doi.org/10.1016/j.apsusc.2020.145425.
30. Xie B., Qin J., Wang S., Li X., Sun H., Chen W. – Adsorption of phenol on commercial activated carbons: Modeling and interpretation. Int. J. Environ. Res. Public Health, **17** (2020) 789. https://doi.org/10.3390/ijerph17030789.
31. Lorenc-Grabowska E. – Effect of micropore size distribution on phenol adsorption on steam activated carbons. Adsorption, **22** (2015) 599–607. https://doi.org/10.1007/s10450-015-9737-x.
32. Hamdaoui O., Naffrechoux E. – Modeling of adsorption isotherms of phenol and chlorophenols onto granular activated carbon, Part I. Two-parameter models and equations allowing determination of thermodynamic parameters. J. Hazard. Mater., **147** (2007) 381–394. https://doi.org/10.1016/j.jhazmat.2007.01.021.